

Characterization of Ionospheric Disturbances Following Multiple Typhoons Using GPS-Derived TEC

Junxian Fu¹  and Shuanggen Jin^{1,2,3} 

¹School of Remote Sensing and Geomatics Engineering, Nanjing University of Information Science and Technology, Nanjing, China, ²School of Surveying and Land Information Engineering, Henan Polytechnic University, Jiaozuo, China, ³Shanghai Astronomical Observatory, Chinese Academy of Sciences, Shanghai, China

Key Points:

- Significant ionospheric disturbances are observed following multiple typhoons from GPS-derived Total Electron Content data
- The directivities of positive and negative ionospheric disturbances are found in different azimuths
- The magnitude of ionospheric disturbances is related to the typhoon intensity with a positive proportion

Correspondence to:

S. Jin,
sgjin@nuist.edu.cn;
sg.jin@yahoo.com

Citation:

Fu, J., & Jin, S. (2023). Characterization of ionospheric disturbances following multiple typhoons using GPS-derived TEC. *Journal of Geophysical Research: Space Physics*, 128, e2022JA030457. <https://doi.org/10.1029/2022JA030457>

Received 11 MAR 2022

Accepted 18 DEC 2022

Author Contributions:

Conceptualization: Junxian Fu
Data curation: Junxian Fu
Formal analysis: Junxian Fu
Investigation: Junxian Fu
Methodology: Junxian Fu
Resources: Junxian Fu
Software: Junxian Fu
Validation: Junxian Fu
Writing – original draft: Junxian Fu

Abstract Typhoon is one of the major hazards in ocean coastal areas, but traditional techniques are inadequate to monitor typhoons due to limited or high-cost observations, like radio sounding and meteorological radar. Previous studies have found that typhoons can cause ionospheric disturbances, but the relationship and characteristics are still unclear. In this paper, about 400 stations observations of the Global Positioning System (GPS) network in Taiwan are used to extract ionospheric disturbances during multiple typhoons. The detailed characteristics of the ionospheric disturbances are investigated using a fourth-order Butterworth filter following the 2016 Nepartak, 2019 Lekima, 2019 Mitag, and 2020 Hagupit typhoons. The results show that significant ionospheric disturbances were observed during the typhoons, and the larger disturbances are mostly located 400–1200 km far from the typhoon eye. The estimated horizontal propagation velocity of the ionospheric disturbances is about 127–194 m/s. The locations of the ionospheric disturbances between the typhoon eye and the landfall site are related to the typhoon path. The azimuth distribution of the ionospheric disturbance around the typhoon eye is affected by the GPS elevation angles. At 500–700 km from the typhoon eye, the mean ionospheric disturbances are 0.17 TECU (TEC Unit) and 0.15 TECU for super typhoon Nepartak and Lekima, and 0.13 TECU and 0.18 TECU for typhoon Mitag and Hagupit. The higher the intensity of the typhoon is, the greater the magnitude of the ionospheric disturbance is.

1. Introduction

Typhoon is a natural disaster with causing large losses and frequently occurs in west pacific regions, and therefore monitoring and predicting typhoons are important. Global Positioning System (GPS) observations provide opportunities for monitoring and studying typhoons because they are more widely distributed and capable of continuous observation than other methods. The relationship between the ionospheric disturbances and the intense atmospheric activities has been found in the foF2 changes (Bauer, 1958) as well as the traveling ionospheric disturbances (Hung et al., 1978; Tsutsui & Ogawa, 1973). There are many claims for the cause of the disturbance, and gravity waves are the main reason (Chernogor et al., 2021, 2022). The acoustic gravity waves caused by the typhoon result in ionospheric disturbances (Tsutsui & Ogawa, 1973). Fritts and Alexander (2003) found that gravity waves not only affect the lower atmosphere but also the middle atmosphere, however, the weak background winds are necessary for the continually upwards propagation of the gravity waves from the top of the troposphere argued by Yue et al. (2009). Although the ionospheric disturbances resulting from the typhoon-triggered gravity waves have been widely accepted, the relationship among them from the observable data is still incomplete.

Due to the low-frequency observations and the sparse stations, it is difficult to obtain intensive and real-time data using traditional methods. The ionospheric delay is one of GPS main errors (Jin et al., 2005; Jin & Su, 2020), and nowadays the Total Electron Content (TEC) can be obtained from dual-frequency GPS observations (Jin et al., 2022; Su et al., 2019), which can be used to determine ionospheric disturbances following earthquakes and typhoons. Earthquakes may cause ionospheric disturbances (Jin et al., 2011), but their horizontal propagation velocity (Cahyadi et al., 2022) and central frequency (Chai & Jin, 2021) are different from those caused by typhoons obviously. During Typhoon Matsa, Mao et al. (2010) found the typhoon affected the ionosphere before landfall, and the effect diminished as the typhoon landed from the ionospheric disturbances. Chou et al. (2017) observed multiple TIDs with periods of 8–30 min triggered by Typhoon Meranti. Song et al. (2019) reported the horizontal propagation velocities of the TIDs were 268 and 143 m/s using the GPS network data of China combined with observations of an ionosonde chain. Interestingly, there was no significant disturbance at the eye of the typhoon, and the disturbance at several stations became greater with the increasing distance to the eye (Wen

Table 1
Typhoon Information

Name	Date of born	Date of landfall	Date of max wind speed	Max wind speed
Nepartak (201,601)	2016.7.3	2016.7.9	2016.7.6	68 m/s
Lekima (201,909)	2019.8.4	2019.8.10	2019.8.8	62 m/s
Mitag (201,918)	2019.9.28	2019.10.1	2019.9.30	40 m/s
Hagupit (202,004)	2020.8.1	2020.8.6	2020.8.3	38 m/s

& Jin, 2020). The typhoon-induced ionospheric disturbances are reaching a maximum at a distance of 1,300 km from the typhoon eye, and are reduced progressively to zero at more than 2100 km (Chen et al., 2020). The variation in the propagation of the disturbance may be related to the propagation loss of gravity waves in the thermosphere (Vadas, 2007), and its propagation speed and period are gradually stabilized within 1,000 km from the typhoon eye (Zhao et al., 2020).

There are obvious differences among the results of the characteristics of typhoon-induced ionospheric disturbances caused by the different chosen typhoons and the coupling relations between typhoons and ionospheric disturbances (Chou et al., 2017; Wen & Jin, 2020). To answer how typhoons

trigger gravity waves and how they propagate through the atmosphere, the ionospheric disturbance characteristics triggered by several typhoons with different intensities and paths should be investigated and analyzed for the relationship between typhoons and ionospheric disturbance.

In this paper, we aim to study the disturbance characteristics following different typhoons near the Taiwan Island during the period of maximal intensity and wind speed. About 400 stations with a sampling interval of 30 s from the Taiwan GPS network are used to obtain the vertical TEC. The ionospheric disturbances triggered by multiple typhoons are extracted from TEC using the fourth-order Butterworth filter. The ionospheric disturbances are estimated during multiple typhoons from GPS-derived TEC. The detailed characteristics and relationship of the ionospheric disturbances are investigated from more typhoons. In the following, data and methods are shown in Section 2, results and analysis are presented in Section 3, and Discussion and conclusions are given in Sections 4 and 5, respectively.

2. Data and Methods

2.1. Data

Data used in our study, including hourly typhoon eye position, moving direction, wind speed, and central pressure, are from National Meteorological Center (NMC, <http://typhoon.nmc.cn/web.html>) (Table 1). According to the typhoon track shown in Figure 1, the Nepartak landed on southern Taiwan and the China mainland successively, while Lekima, Mitag, and Hagupit landed after passing through the waters of northern Taiwan. The GPS data with a sampling interval of 30 s are from Central Weather Bureau (CWB), Taiwan. The data from about 400 stations were used in this study.

In this paper, four typhoons are selected for analysis, and the information of the typhoons is shown in Table 1.

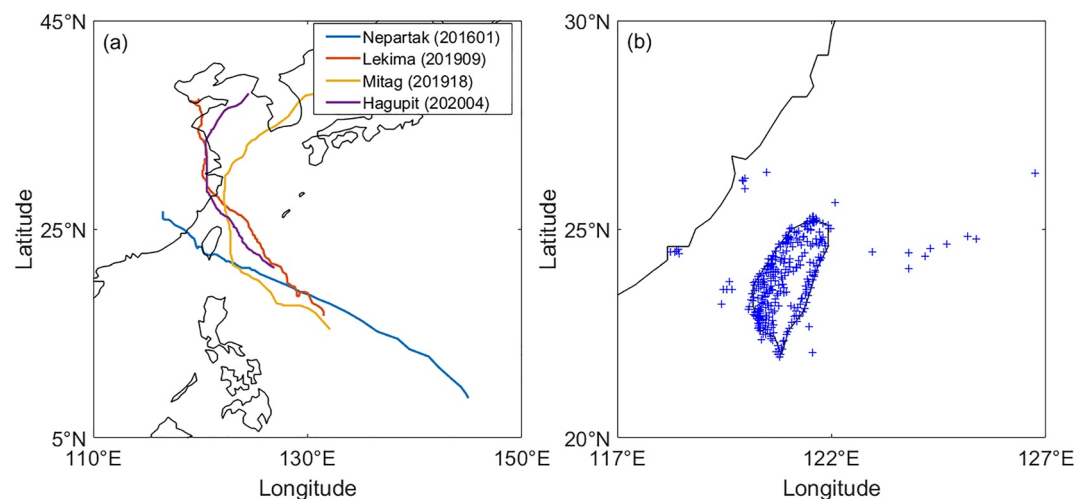


Figure 1. (a) Typhoon tracks and (b) distribution of the Global Positioning System stations.

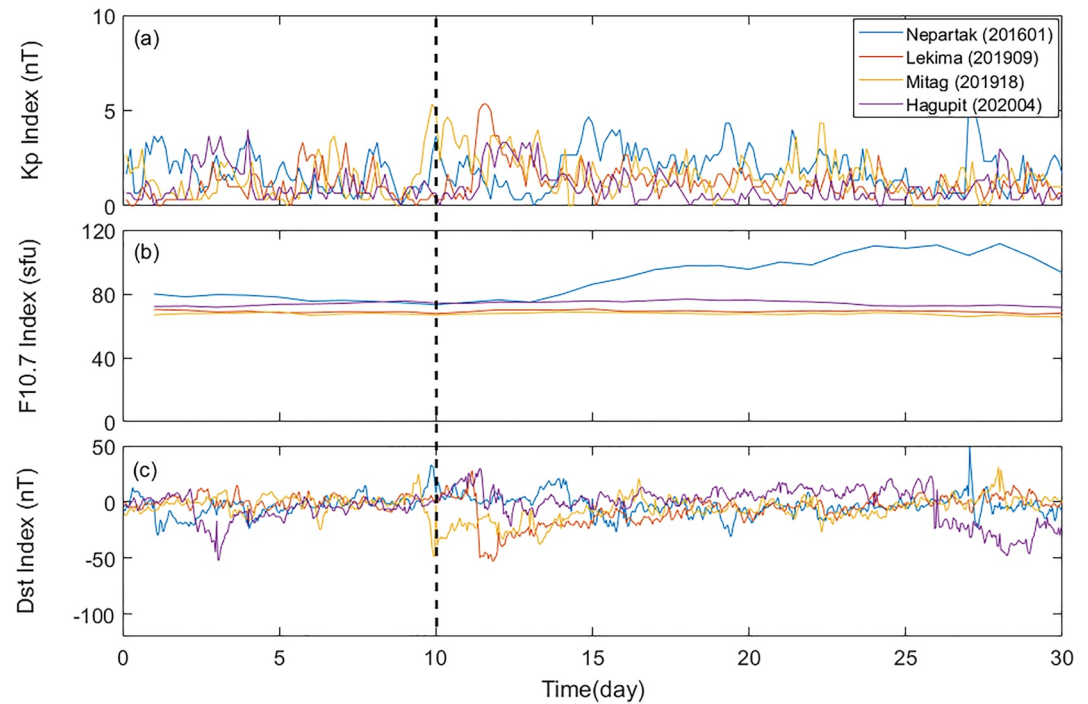


Figure 2. Time series of Kp index (a), F10.7 index (b), and Dst index (c).

Since solar and geomagnetic activities affect the ionosphere, their possible impacts on typhoon-induced ionospheric disturbances should be eliminated or reduced. The intensity of solar and geomagnetic activity can be illustrated by three indexes. The Kp index and the Dst index are used to describe the geomagnetic activity, and the solar radiation F10.7 index is used to describe the solar activity. Kp index and F10.7 index are obtained from the German Research Centre for Geosciences (GFZ, <https://www.gfz-potsdam.de/en/kp-index/>), and the Dst index data are from the World Data Center (ICSU-WDS, <http://wdc.kugi.kyoto-u.ac.jp/wdc/Sec3.html>). Figure 2 shows the time sequences of the Kp index, F10.7 index, and Dst index within 30 days from 10 days before the typhoon generation date. During the study periods, the Kp index exceeds 4 nT only in a few periods, the F10.7 index is between 60 and 100 sfu, and the Dst index is greater than -30 nT, so the solar and geomagnetic activities are considered to be calm (Liu & Jin, 2019).

2.2. Methods

It is assumed that all free electrons are concentrated on a thin spherical shell at a certain altitude. The intersection of the satellite to the GPS receiver line is defined as the ionosphere pierce point (IPP). The latitude and longitude of IPP can be obtained based on the position of the satellite and the measurement station. In this method, the variations of TEC are assumed to occur on the IPP. Slant TEC (STEC) can be obtained from dual-frequency observations (Jin et al., 2014):

$$\begin{aligned} \text{STEC} &= \frac{f_1^2 f_2^2}{40.3(f_1^2 - f_2^2)} (L_1 - L_2 + \lambda_1(N_1 + b_1) - \lambda_2(N_2 + b_2) + \epsilon) \\ &= \frac{f_1^2 f_2^2}{40.3(f_1^2 - f_2^2)} (P_1 - P_2 - (d_1 - d_2) + \epsilon) \end{aligned} \quad (1)$$

where f is the carrier phase frequency, $f_1 = 1,575.42$ MHz and $f_2 = 1,227.60$ MHz, L and P are the carrier phase and pseudorange observations, respectively, b and d are the instrumental errors of the carrier phase and pseudorange, and ϵ are the residuals. In a continuous observation, N_1 and N_2 are fixed values, while ambiguity, differential code biases, and noises are estimated as constant (Jin et al., 2017). Then the constant terms are removed by low-frequency filtering and the precise TEC can be obtained.

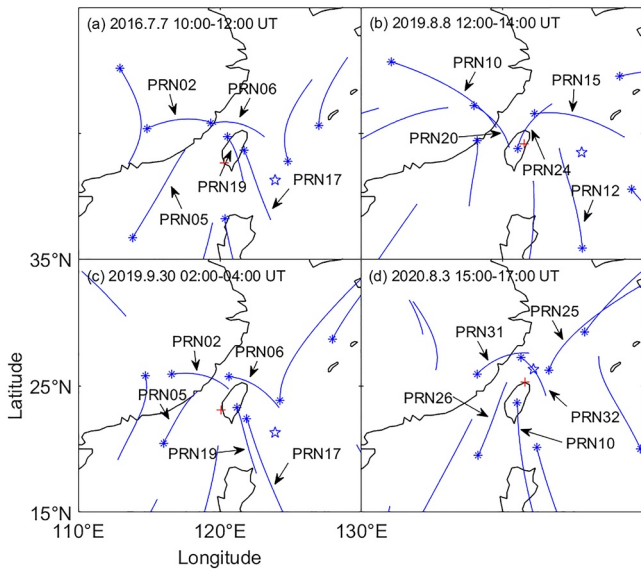


Figure 3. Ionosphere pierce point tracks of typhoon (a) Nepartak, (b) Lekima, (c) Mitag, and (d) Hagupit. The red cross shows the location of the station, and the blue pentagram is the location of the typhoon eye in the middle of the selected period. Pseudo Random Noise means the serial number of the satellite. Two hours were chosen during each typhoon around the maximal intensity and wind speed.

The slant TEC is converted into vertical TEC by:

$$VTEC = STEC * \cos\left(\arcsin\left(\frac{R \sin z}{R + H}\right)\right) \quad (2)$$

where R is the radius of the Earth (6,371 km), and H is the assumed height of the ionospheric spherical shell, which is set as the mean 350 km of the F region peak height (Song et al., 2019), and z is the satellite elevation angle.

Before estimating TEC from dual-frequency observations, the effect of cycle slips needs to be eliminated. In this paper, the detection and repair of the cycle slips are performed by the second-order, time-difference phase ionospheric residual method (Cai et al., 2013). The typhoon-induced ionospheric disturbance can be obtained from the relative changes of TEC. To extract significant ionospheric disturbance, the fourth-order Butterworth filter (Jin et al., 2014) was used to remove the effects caused by IPPs motion and ionospheric background variations from the TEC. For example, we detect signals smaller than 16.7 mHz based on Nyquist's theorem GPS observations with a sampling interval of 30 s. Also, 1 mHz is chosen as the cutoff value to eliminate the variation of the background TEC. The filtering results show that the amplitude of the extracted ionospheric disturbances is most obvious when the cutoff frequency is 1–3 mHz, which is related to the gravity wave frequency range.

3. Results and Analysis

The tracks of IPPs are similar for the same satellite observed by different stations in the same period, so the result of one station can show the movements of IPPs (Figure 3).

During the study period, obvious ionospheric disturbances are observed following the multiple typhoons from GPS TEC. The error of TEC is estimated with about 0.1 TECU. Figure 4 shows TEC disturbances at several stations during the typhoon from the filtered TECs in the range of 0.1–0.2 TECU, while the characteristics of the disturbances were different. During Typhoon Lekima, the disturbances were close to 0.2 TECU observed by station CISH and GS07 for satellite PRN20, while about 0.1 TECU is observed by station DOSE and FUNY for satellite PRN24. To show the significance of TEC disturbances, we have calculated the root mean square of the TEC disturbance time series, whose sigma is about 0.02 TECU (e.g., 2019 Lekima Typhoon), and most disturbances are over 3 times of sigma, which is significant at 99.7% confidence level.

3.1. Propagation Direction and Velocity of Ionospheric Disturbances

Figure 5 shows the distribution of ionospheric punctures of the four typhoons with multiple satellites. In Figure 5a, during the period from 10:00 UT to 12:00 UT on 7 July 2016, Nepartak was a super typhoon. The ionospheric punctures of PRN02 and PRN06 were located northwest of the typhoon eye, and obvious ionospheric disturbances were observed, while the disturbances detected by the IPPs of PRN17 and PRN09 during this period were not obvious. The disturbances observed by several satellites are mainly in the western and northwestern directions of the typhoon eye. Figure 5b shows the ionospheric disturbance of Typhoon Lekima at 13:05 UT on 8 August 2019. During the period from 12:00 UT to 14:00 UT, the disturbances detected by PRN20 and PRN24 were mainly distributed in the western direction of the typhoon center, while no significant disturbances were observed in the southern and northern directions of the typhoon eye. Figure 5c shows Typhoon Mitag at 02:53 UT on 30 September 2019. During the period from 02:00 UT to 04:00 UT, ionospheric disturbances were detected by PRN02, PRN05, and PRN06, which are located northwest of the typhoon eye. In Figure 5d, the ionospheric disturbances of Typhoon Hagupit were detected at PRN25 in the east direction and PRN31 in the west direction of the typhoon eye at 15:50 UT on 3 August 2020. These results show that the observations from different satellites are inconsistent.

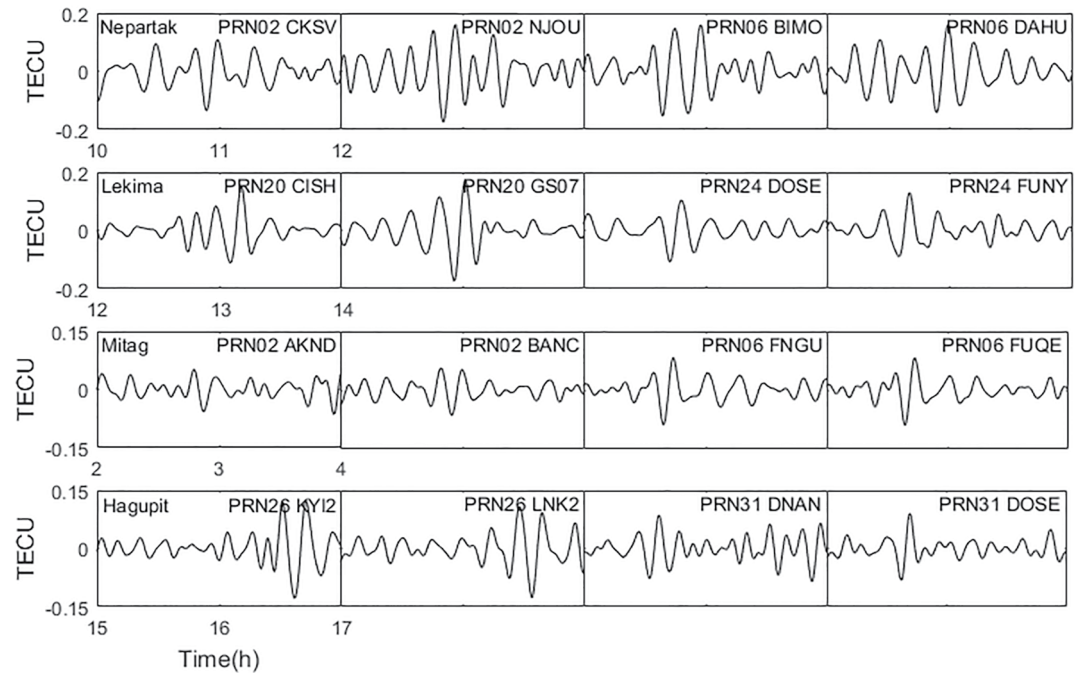


Figure 4. Total Electron Content variations at different stations following the Nepartak, Lekima, Mitag, and Hagupit typhoons.

The direction of the disturbance propagation can be detected by the variation of the disturbance at IPPs at different times. The source location of the ionospheric disturbance can be conjectured using observations from multiple satellites, such as the western and northwestern directions observed by the satellites PRN02 and PRN06 (Figure 5a), suggesting that the source of the ionospheric disturbance of Typhoon Nepartak is located near the typhoon eye. During the selected period, the ionospheric disturbance sources of Typhoon Nepartak and Mitag were located close to the typhoon center, while that for Typhoon Lekima and Hagupit were located roughly northwest of the typhoon eye. The difference in the source locations may be related to the track of the typhoon during this period.

The distribution of the extremum of the disturbances observed by several satellites during the study period is shown in Figure 6. In terms of the results, the satellite elevation angle at the IPP about 600 km away from the typhoon center, where significant disturbances were observed for the four typhoons, is concentrated around 45° – 60° . This suggests that the satellite elevation angle may affect the observation of disturbances. Higher intensity typhoons seem to less likely observe large disturbances in areas close to the typhoon eye.

The propagation velocity of the ionospheric disturbance can be estimated from the distance between the IPP and the typhoon eye and the filtered ionospheric disturbance. The horizontal propagation velocities of the ionospheric disturbance triggered by Typhoon Nepartak, Lekima, Mitag, and Hagupit are about 191, 194, 144, and 127 m/s, respectively (Figure 7). The propagation velocities of the ionospheric disturbances triggered by these four typhoons are in the range of the signal propagation velocity when the gravity waves are coupled with the ionosphere. Using the Short Time Fourier Transform to transform the filtered TEC from the time domain to the frequency domain, the central frequency of the disturbance can be obtained at about 1.6 mHz, which is consistent with the signal frequency of gravity waves coupled with the ionosphere (Jin et al., 2015), suggesting that these disturbances are triggered by typhoon-excited gravity waves.

3.2. Relationship Between Disturbance Amplitude and Typhoon Strength

Several studies (Chen et al., 2020; Wen & Jin, 2020) have shown that the magnitude of ionospheric disturbances was related to the distance between the IPP and the typhoon eye, but only a small number of stations have been used for comparison. Figure 8 shows the distribution of the magnitude and distance of the disturbances from

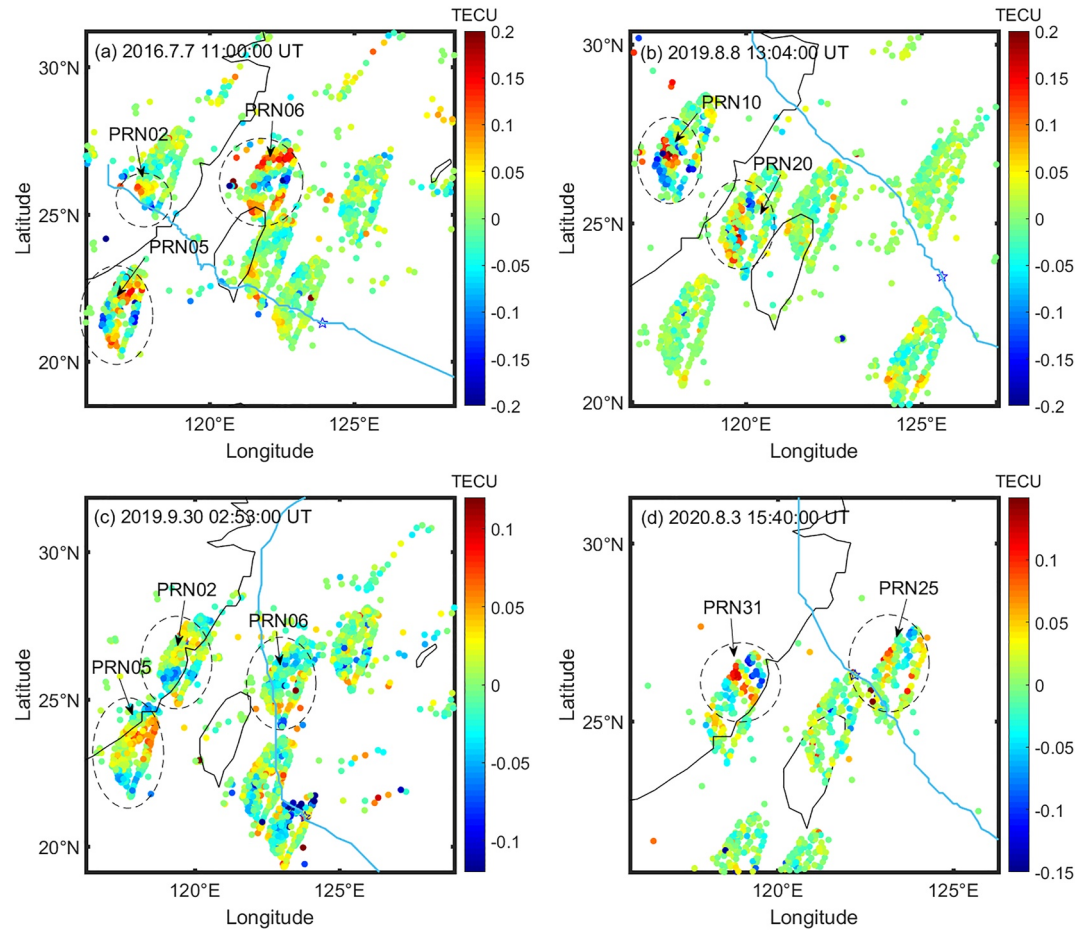


Figure 5. IPPs distribution of (a) Nepartak; (b) Lekima; (c) Mitag; and (d) Hagupit. The blue pentagram represents the location of the typhoon eye. The blue lines mean the typhoon tracks.

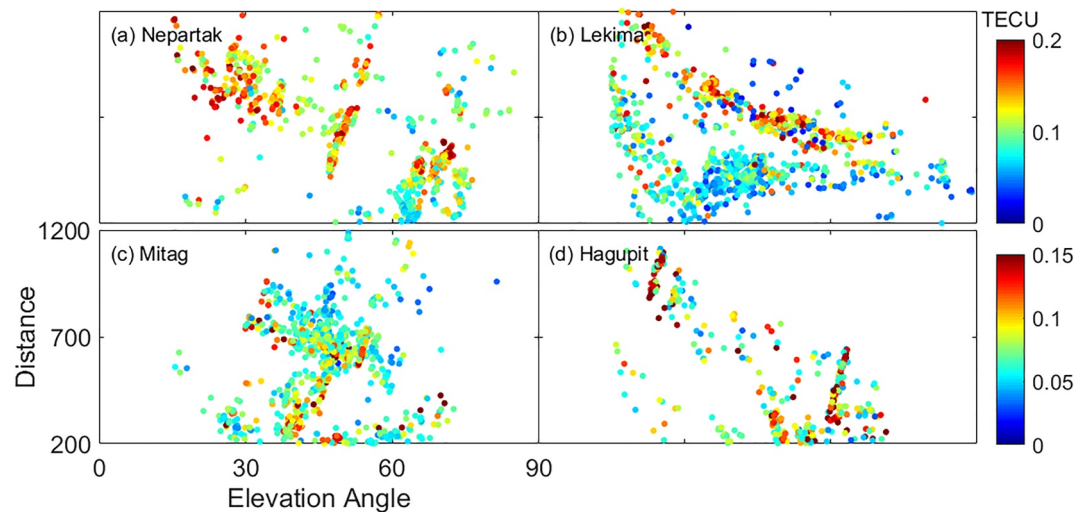


Figure 6. The magnitude of the ionospheric disturbances.

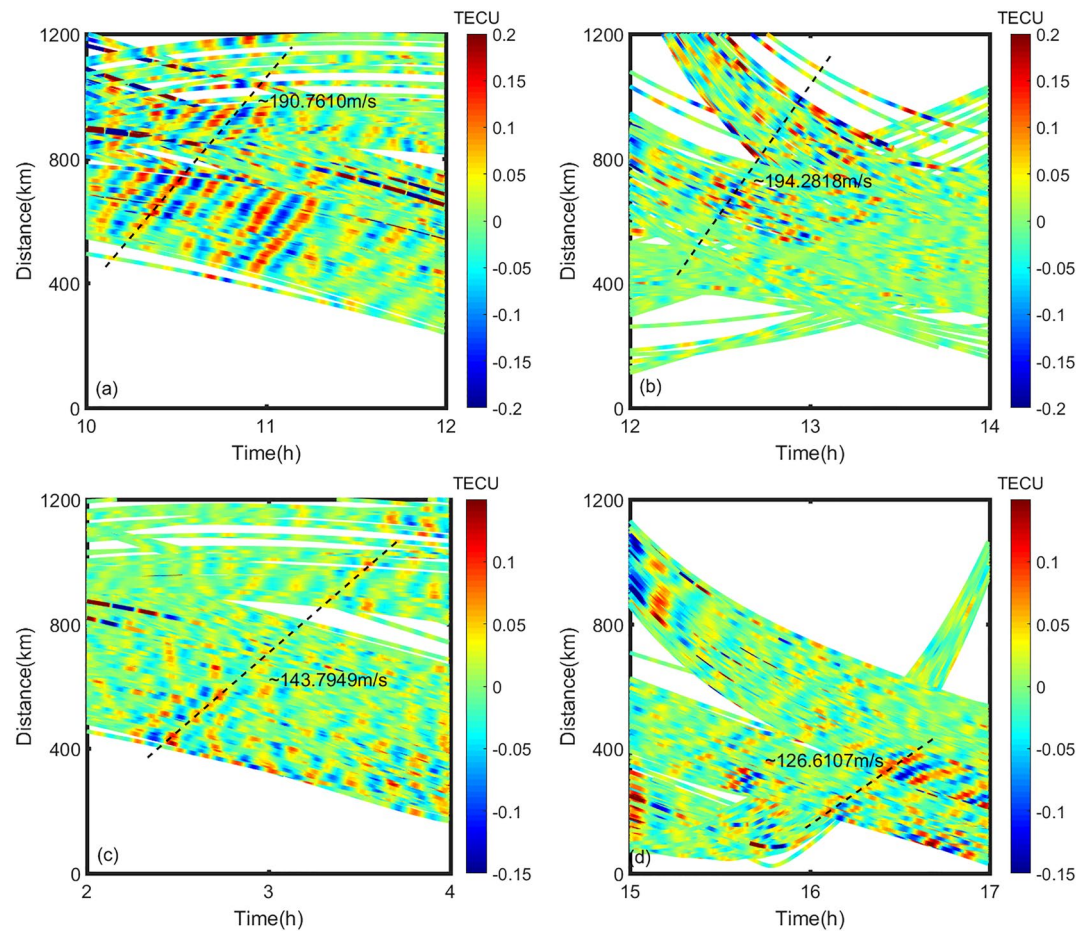


Figure 7. The variation of the disturbance size and distance with the time for (a) Nepartak; (b) Lekima; (c) Mitag; and (d) Hagupit. The black dashed line is used to fit the disturbance propagation speed.

multiple stations during four typhoons. The color dots show the relationship between the extreme magnitude of the disturbance and the distance between the IPP and the typhoon center during the study period.

The statistical results show that the mean value of the disturbance is 0.1180 TECU for PRN02 and 0.1383 TECU for PRN06 during Typhoon Nepartak, and the distance between the IPP of PRN02 and the typhoon eye is farther than that of PRN06. This indicates that the disturbance is greater at a more distant location from the typhoon eye. This is also confirmed by Typhoon Lekima shown in Figure 8b, where the magnitude of the disturbance is 0.1435 TECU for PRN20 and 0.1331 TECU for the closer PRN24. The disturbance magnitude is 0.1228 TECU for PRN05 and 0.1156 TECU for PRN06, while the number of stations during Typhoon Hagupit in Figure 8d is small, and the disturbance magnitudes of PRN26 and PRN31 are 0.1321 TECU and 0.1007 TECU, respectively.

To reduce the effect of the distance, the ionospheric disturbances observed between 500 and 700 km from the typhoon eye were selected to analyze the relationship between disturbance magnitude and typhoon intensity. The mean values of the ionospheric disturbance during the study period are linearly fitted to the maximum wind speeds of the four typhoons. The results show that the mean values of the disturbance triggered by Typhoon Nepartak, Lekima, Mitag, and Hagupit are 0.1676 TECU, 0.1495 TECU, 0.1338 TECU, and 0.1755 TECU, respectively. Combined with the data of Typhoon Hato and typhoon Meranti, the fitting results of the six-typhoon ionospheric disturbances are shown in Figure 9, which shows a good linear relationship between the ionospheric disturbance magnitude and the typhoon intensity.

The results show a good correlation between the magnitude of ionospheric disturbances and the typhoon wind speed. The higher the typhoon intensity is, the larger the disturbance magnitude is. However, the number of stations in this study was around 400 for the typhoons Mitag, Lekima, Nepartak, and Meranti, while about 140

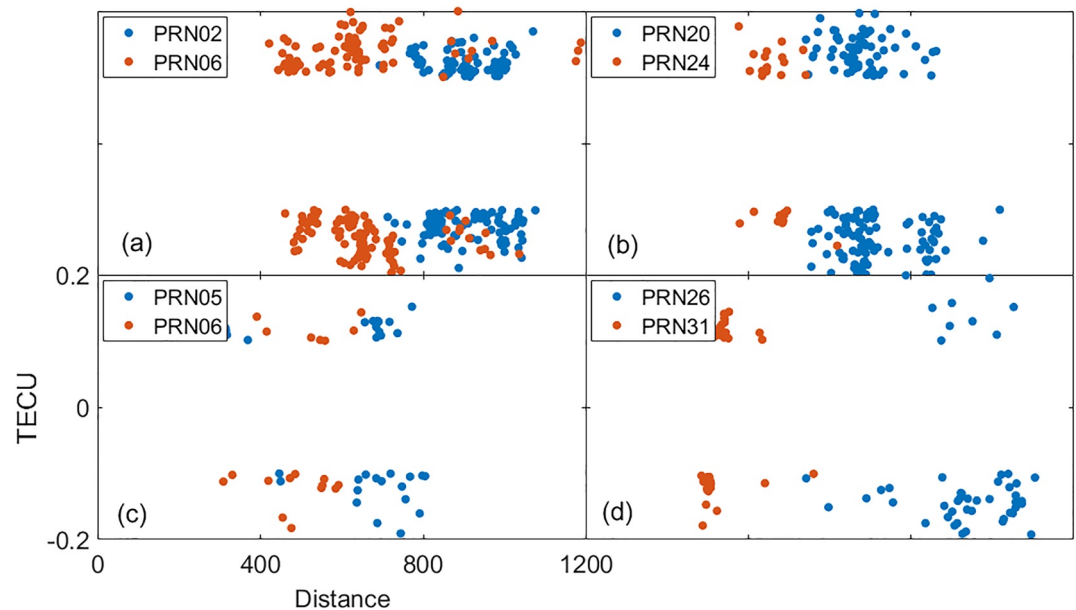


Figure 8. The relationship between the extreme magnitude of the disturbance and the distance between the ionosphere pierce point and the typhoon eye during the study period for (a) Nepartak; (b) Lekima; (c) Mitag; and (d) Hagupit.

for typhoons Hagupit and Hato. A more accurate relationship should be further studied with more typhoons by the same stations.

3.3. Distribution of Positive and Negative Disturbances

From the results, it is clear that there are not only differences in the magnitude of the ionospheric disturbances triggered by the typhoon, but also inconsistencies between the positive and negative anomalies of the disturbances. As can be seen from Figure 10a, the disturbances observed at stations PR11, DOSE, DOJ1, and DNAN through PRN31 are negative first, that is, inverted-N type. While the disturbances observed by the stations STA1 and PAO2 through PRN25, the first two stations show positive disturbances first and then negative disturbances, that is, N-type, but LIY2 and CHUA are inverted N type. As shown in Figures 10b and 10c, PRN31, which is located in the west direction of the typhoon center, has a more obvious positive and negative disturbance distribution when compared with PRN25 in the east direction.

Figure 11 shows the distribution of positive and negative ionospheric disturbances of four typhoons. The number of IPPs with first positive disturbances for these four typhoons is 416, 303, 137, and 164, while the number of IPPs with first negative disturbances is 462, 426, 296, and 135. It is not significantly different in number, but the results appear that the positive or negative disturbances are more concentrated in some areas.

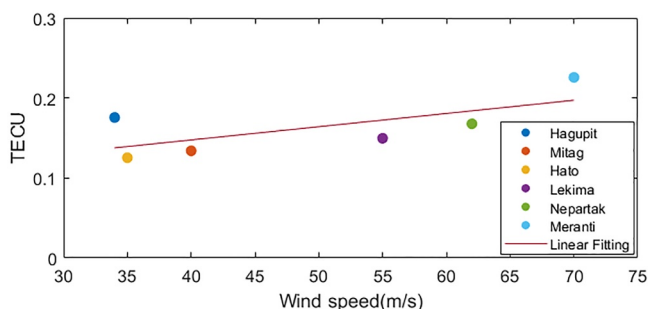


Figure 9. The relationship between disturbance magnitude and typhoon intensity.

4. Discussion

Ionospheric disturbances triggered by typhoon-excited gravity waves were observed during the approaching landfall of several typhoons. Through the analysis of the characteristics of ionospheric disturbances triggered by several typhoons, it is found that the ionospheric disturbance characteristics are closely related to the typhoon path, intensity, and other factors. However, for finding the pattern between typhoons and ionospheric disturbances, there are still several problems to be solved as follows.

The mechanism of typhoon-induced disturbances is still unclear, for example, the sources of the disturbances observed during the study period for Typhoon

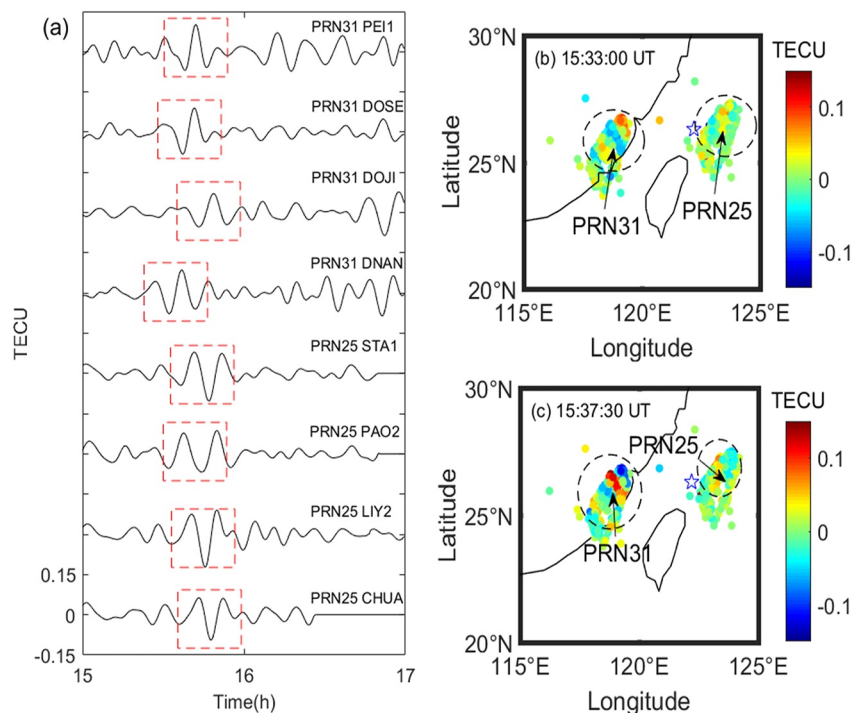


Figure 10. (a) The Total Electron Content time series of PRN25 and PRN31 at different stations during Typhoon Hagupit. The red rectangle shows the observed ionospheric disturbances; (b) and (c) are TEC disturbances at ionosphere pierce points with different times.

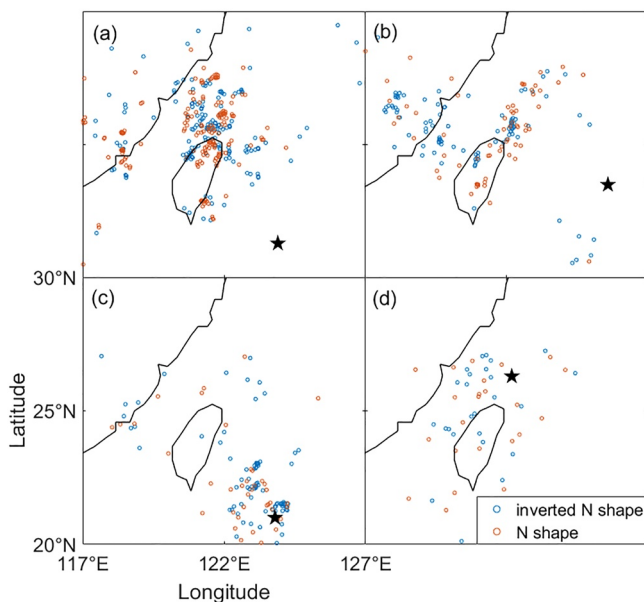


Figure 11. The distribution of positive and negative ionospheric disturbances for (a) Nepartak; (b) Lekima; (c) Mitag; and (d) Hagupit. The red IPPs are positively observed first, the blue ionosphere pierce points are negatively observed first, and the black pentagrams are the locations of the typhoon eyes at this time.

Nepartak and Mitag in Figure 5 are located near the typhoon eye, while the sources of Typhoon Lekima and Hagupit are located northwest of the typhoon eye. This may be related to the typhoon's path, as Typhoon Nepartak and Mitag are located in the east of Taiwan and moving toward Taiwan, while Typhoon Lekima and Hagupit are located in the north of Taiwan and moving toward the mainland. According to Kong et al. (2017), this was because the typhoon covered the mountainous area with strong winds before landfall, and the violently undulating topography allowed gravity waves to propagate into the ionosphere. But this cannot explain the observation that the disturbance source is located near the typhoon eye in this study.

On the other hand, Vadas and Fritts (2009) showed that gravity waves propagated upward as concentric rings in the isothermal, windless middle and lower atmosphere, and later Yue et al. (2009) observed near-perfect concentric rings triggered by gravity waves at 87 km altitude using the all-sky OH imager. The IPP height was set to 350 km, and the actually observed disturbances located in different directions at the typhoon center did not show a ring shape, which were inconsistent with the results of the previous studies (Vadas & Fritts, 2009; Yue et al., 2009). As is shown in Figure 5, significant disturbances are not observed in all directions of the typhoon center. In this regard, this was the result of gravity waves reaching the ionosphere after breaking and absorption in the stratosphere and mesosphere, according to Chou et al. (2017). Kong et al. (2017) also suggested that gravity waves would not be able to propagate freely due to the breaking of gravity waves, absorption in the critical layer, and reflection in the stratosphere. Zhao et al. (2020) speculated that this could be caused by changes in the background wind and the influence of the magnetic field, due to the propagation anisotropy of

the ionospheric disturbances regarding the magnetic inclination (Heki & Ping, 2005; Song et al., 2017), and Freeshah et al. (2021) proposed the effect that the meridional wind may affect the coupling of the atmosphere and ionosphere.

The observation of disturbances is influenced by a number of factors. For example, the satellite elevation angle also affects the observation of disturbances (Figure 6), since the TEC are most sensitive to the perpendicular disturbances along the line of sight (Jin, 2018). The disturbances may be more easily observed at some elevation angles due to the slant propagation up to the ionosphere of the gravity waves (Li et al., 2018). When the wave path and satellite line of sight are parallel to each other, the integration of wavefronts cancels the wave phases and thus results in minimal amplitudes (Bagiya et al., 2017). The amplitude of disturbances also shows differences under different methods (Zheng et al., 2022), the variations in the electron density are 3%–19%, while the disturbances in this study are less than 1%. This difference is most likely due to the “smoothing out” (Xu et al., 2019). If the vertical wavelengths of disturbance are smaller than the F layer thickness, the amplitudes are expected to be significantly reduced in this study. The filtering, the distance between IPP and typhoon eye, the disturbance period, etc., also affect the amplitude of disturbances. This is related to the dissipation of AGWs in propagation (Chen et al., 2020; Vadas, 2007). The propagation of gravity waves in the atmosphere and the coupling process in the ionosphere remain unclear due to the continuous decay of the atmospheric density, which propagates in a nonlinear manner. The trajectories of the ionospheric punctures during the study period are shown in Figure 3, and the ionospheric punctures only cover part of the area near the typhoon center as shown in Figure 5. More simultaneous observations of the satellites can obtain more comprehensive ionospheric punctures with covering all directions of the typhoon center and thus obtain more detailed disturbance characteristics.

Although the relationship between the magnitude of ionospheric disturbances and the typhoon intensity is found for six typhoons, more case studies are needed under the same conditions, such as the same filtering methods, satellite elevations, and coverages. The clear positive and negative ionospheric perturbations are observed in different directions of the typhoon eye, which needs to further study the possible reasons.

5. Conclusions

In this paper, the ionospheric disturbances caused by four typhoons are analyzed and investigated by using GPS observations at about 400 stations from the dense continuous GPS observation network in Taiwan with a sampling interval of 30 s. The ionospheric disturbances following four typhoons are extracted from TEC using a fourth-order Butterworth filter. The main results are summarized as.

1. Significant ionospheric disturbances were observed from GPS-derived TEC data following 2016 Nepartak, 2019 Lekima, 2019 Mitag, and 2020 Hagupit typhoons.
2. The mean ionospheric disturbance amplitudes are 0.1676 and 0.1495 TECU for the super typhoon Nepartak and Lekima, and 0.1338, and 0.1755 TECU for the typhoon Mitag and Hagupit, which are correlated to the intensity and maximum wind speed of the typhoon. The higher the intensity of the typhoon is, the greater the magnitude of the ionospheric disturbance is.
3. The positive and negative ionospheric disturbances are distributed in different directions of the typhoon eyes. During typhoon Hagupit, most negative disturbances were observed first at the ionospheric penetration point of PRN31, which is located in the western direction of the typhoon eye. More positive disturbances were observed first at PRN25, which is located in the eastern direction of the typhoon eye.

Data Availability Statement

The typhoon data used in the study are available at National Meteorological Centre (NMC, <http://typhoon.nmc.cn/web.html>). The GPS data used for TEC extraction in the study are from Central Weather Bureau (CWB), Taiwan. Kp index and F10.7 index in the study are obtained from the German Research Centre for Geosciences (GFZ, <https://www.gfz-potsdam.de/en/kp-index/>), and the Dst index data from the World Data Center (ICSU-WDS, <http://wdc.kugi.kyoto-u.ac.jp/wdc/Sec3.html>).

Acknowledgments

The work was supported by the National Natural Science Foundation of China (NSFC) Project (Grant 12073012) and the authors thank the Taiwan Central Weather Bureau (CWB) for providing the GNSS data.

References

- Bagiya, M. S., Sunil, A. S., Sunil, P. S., Sreejith, K. M., Rolland, L., & Ramesh, D. S. (2017). Efficiency of coseismic ionospheric perturbations in identifying crustal deformation pattern: Case study based on Mw 7.3 May Nepal 2015 earthquake. *Journal of Geophysical Research: Space Physics*, 122(6), 6849–6857. <https://doi.org/10.1002/2017JA024050>
- Bauer, S. J. (1958). An apparent ionospheric response to the passage of hurricanes. *Journal of Geophysical Research*, 63(1), 265–269. <https://doi.org/10.1029/jz063i001p00265>
- Cahyadi, M., Muslim, B., Pratomo, D., Anjasmara, I., Arisa, D., Rahayu, R., et al. (2022). Co-seismic ionospheric disturbances following the 2016 West Sumatra and 2018 Palu earthquakes from GPS and GLONASS measurements. *Remote Sensing*, 14(2), 401. <https://doi.org/10.3390/rs14020401>
- Cai, C., Liu, Z., Xia, P., & Dai, W. (2013). Cycle slip detection and repair for undifferenced gps observations under high ionospheric activity. *GPS Solutions*, 17(2), 247–260. <https://doi.org/10.1007/s10291-012-0275-7>
- Chai, Y., & Jin, S. G. (2021). Two-azimuth co-seismic ionospheric disturbances following the 2020 Jamaica earthquake from GPS observations. *Journal of Geophysical Research: Space Physics*, 126(9), e2020JA028995. <https://doi.org/10.1029/2020JA028995>
- Chen, J., Zhang, X., Ren, X., Zhang, J., & Zhao, Z. (2020). Ionospheric disturbances detected during a typhoon based on GNSS phase observations: A case study for typhoon mangkhut over Hong Kong. *Advances in Space Research*, 66(7), 1743–1753. <https://doi.org/10.1016/j.asr.2020.06.006>
- Chernogor, L. F., Garmash, K. P., Guo, Q., Rozumenko, V. T., Zheng, Y., & Luo, Y. (2021). Super typhoon Hagibis action in the ionosphere on 6–13 October 2019: Results from multi-frequency multiple path sounding at oblique incidence. *Advances in Space Research*, 67(8), 2439–2469. <https://doi.org/10.1016/j.asr.2021.01.038>
- Chernogor, L. F., Garmash, K. P., Guo, Q., Rozumenko, V. T., Zheng, Y., & Luo, Y. (2022). Disturbances in the ionosphere that accompanied typhoon activity in the vicinity of China in September 2019. *Radio Science*, 57(4), e2022RS007431. <https://doi.org/10.1029/2022RS007431>
- Chou, M. Y., Lin, C. C. H., Yue, J., Tsai, H. F., Sun, Y. Y., Liu, J. Y., & Chen, C. H. (2017). Concentric traveling ionosphere disturbances triggered by Super Typhoon Meranti (2016). *Geophysical Research Letters*, 44(3), 1219–1226. <https://doi.org/10.1002/2016GL072205>
- Freeshah, M., Zhang, X., Sentürk, E., Adil, M. A., Mousa, B. G., Tariq, A., et al. (2021). Analysis of atmospheric and ionospheric variations due to impacts of super typhoon mangkhut (1822) in the northwest Pacific ocean. *Remote Sensing*, 13(4), 661. <https://doi.org/10.3390/rs13040661>
- Fritts, D. C., & Alexander, M. J. (2003). Gravity wave dynamics and effects in the middle atmosphere. *Reviews of Geophysics*, 41(1), 1003. <https://doi.org/10.1029/2001rg000106>
- Heki, K., & Ping, J. (2005). Directivity and apparent velocity of the coseismic ionospheric disturbances observed with a dense GPS array. *Earth and Planetary Science Letters*, 236(3–4), 845–855. <https://doi.org/10.1016/j.epsl.2005.06.010>
- Hung, R. J., Phan, T., & Smith, R. E. (1978). Observation of gravity waves during the extreme tornado outbreak of 3 April 1974. *Journal of Atmospheric and Terrestrial Physics*, 40(7), 831–843. [https://doi.org/10.1016/0021-9169\(78\)90033-8](https://doi.org/10.1016/0021-9169(78)90033-8)
- Jin, S. G. (2018). Two-mode ionospheric disturbances following the 2005 Northern California offshore earthquake from GPS measurements. *Journal of Geophysical Research: Space Physics*, 123(10), 8587–8598. <https://doi.org/10.1029/2017JA025001>
- Jin, S. G., Han, L., & Cho, J. (2011). Lower atmospheric anomalies following the 2008 wenchuan earthquake observed by GPS measurements. *Journal of Atmospheric and Solar-Terrestrial Physics*, 73(7–8), 810–814. <https://doi.org/10.1016/j.jastp.2011.01.023>
- Jin, S. G., Jin, R., & Kutoglu, H. (2017). Positive and negative ionospheric responses to the March 2015 geomagnetic storm from BDS observations. *Journal of Geodesy*, 91(6), 613–626. <https://doi.org/10.1007/s00190-016-0988-4>
- Jin, S. G., Jin, R., & Li, J. H. (2014). Pattern and evolution of seismo-ionospheric disturbances following the 2011 Tohoku earthquakes from GPS observations. *Journal of Geophysical Research: Space Physics*, 119(9), 7914–7927. <https://doi.org/10.1002/2014JA019825>
- Jin, S. G., Occhipinti, G., & Jin, R. (2015). GNSS ionospheric seismology: Recent observation evidences and characteristics. *Earth-Science Reviews*, 147, 54–64. <https://doi.org/10.1016/j.earscirev.2015.05.003>
- Jin, S. G., & Su, K. (2020). PPP models and performances from single-to quad-frequency BDS observations. *Satellite Navigation*, 1(1), 16. <https://doi.org/10.1186/s43020-020-00014-y>
- Jin, S. G., Wang, J., & Park, P. (2005). An improvement of GPS height estimates: Stochastic modeling. *Earth Planets and Space*, 57(4), 253–259. <https://doi.org/10.1186/BF03352561>
- Jin, S. G., Wang, Q., & Dardanelli, G. (2022). A review on multi-GNSS for Earth observation and emerging applications. *Remote Sensing*, 14(16), 3930. <https://doi.org/10.3390/rs14163930>
- Kong, J., Yao, Y., Xu, Y., Kuo, C., Zhang, L., Liu, L., & Zhai, C. (2017). A clear link connecting the troposphere and ionosphere: Ionospheric responses to the 2015 typhoon Dujuan. *Journal of Geodesy*, 91(3), 1087–1097. <https://doi.org/10.1007/s00190-017-1011-4>
- Li, W., Yue, J., Wu, S., Yang, Y., Li, Z., Bi, J., & Zhang, K. (2018). Ionospheric responses to typhoons in Australia during 2005–2014 using GNSS and formasat-3/cosmic measurements. *GPS Solutions*, 22(3), 1–11. <https://doi.org/10.1007/s10291-018-0722-1>
- Liu, Y. H., & Jin, S. G. (2019). Ionospheric Raleigh wave disturbances following the 2018 Alaska earthquake from GPS observations. *Remote Sensing*, 11(8), 901. <https://doi.org/10.3390/rs11080901>
- Mao, T., Wang, J. S., Yang, G. L., Yu, T., Ping, J. S., & Suo, Y. C. (2010). Effects of typhoon matsu on ionospheric tec. *Chinese Science Bulletin*, 55(8), 712–717. <https://doi.org/10.1007/s11434-009-0472-0>
- Song, Q., Ding, F., Zhang, X., Liu, H., Wang, Y., & Zhao, X. (2019). Medium-scale traveling ionospheric disturbances induced by typhoon Chan-hom over China. *Journal of Geophysical Research: Space Physics*, 124(12), 2223–2237. <https://doi.org/10.1029/2018JA026152>
- Song, Q., Ding, F., Zhang, X., & Mao, T. (2017). GPS detection of the ionospheric disturbances over China due to impacts of Typhoons Ramma-sum and Matmo. *Journal of Geophysical Research: Space Physics*, 122(1), 1055–1063. <https://doi.org/10.1002/2016JA023449>
- Su, K., Jin, S. G., & Hoque, M. (2019). Evaluation of ionospheric delay effects on multi-GNSS positioning performance. *Remote Sensing*, 11(2), 171. <https://doi.org/10.3390/rs11020171>
- Tsutsui, M., & Ogawa, T. (1973). HF Doppler observation of ionospheric effects due to typhoons.
- Vadas, S. L. (2007). Horizontal and vertical propagation and dissipation of gravity waves in the thermosphere from lower atmospheric and thermospheric sources. *Journal of Geophysical Research*, 112(A6), A06305. <https://doi.org/10.1029/2006ja011845>
- Vadas, S. L., & Fritts, D. C. (2009). Reconstruction of the gravity wave field from convective plumes via ray tracing. *Annales Geophysicae*, 27(1), 147–177. <https://doi.org/10.5194/angeo-27-147-2009>
- Wen, Y. D., & Jin, S. G. (2020). Traveling ionospheric disturbances characteristics during the 2018 Typhoon Maria from GPS observations. *Remote Sensing*, 12(4), 746. <https://doi.org/10.3390/rs12040746>
- Xu, S., Yue, J., Xue, X., Vadas, S. L., Miller, S. D., Azeem, I., et al. (2019). Dynamical coupling between hurricane Matthew and the middle to upper atmosphere via gravity waves. *Journal of Geophysical Research: Space Physics*, 124(5), 3589–3608. <https://doi.org/10.1029/2018ja026453>

- Yue, J., Vadas, S. L., Chiao, Y., Nakamura, T., Reising, S. C., Liu, H. L., et al. (2009). Concentric gravity waves in the mesosphere generated by deep convective plumes in the lower atmosphere near Fort Collins, Colorado. *Journal of Geophysical Research*, *114*(D6), D06104. <https://doi.org/10.1029/2008JD011244>
- Zhao, Y., Deng, Y., Wang, J. S., Zhang, S. R., & Lin, C. Y. (2020). Tropical cyclone-induced gravity wave perturbations in the upper atmosphere: Gt-m-r simulations. *Journal of Geophysical Research: Space Physics*, *125*(7), e2019JA027675. <https://doi.org/10.1029/2019JA027675>
- Zheng, Y., Chernogor, L. F., Garmash, K. P., Guo, Q., Rozumenko, V. T., & Luo, Y. (2022). Disturbances in the ionosphere and distortion of radio wave characteristics that accompanied the super typhoon Lekima event of 4–12 August 2019. *Journal of Geophysical Research: Space Physics*, *127*(8), e2022JA030553. <https://doi.org/10.1029/2022JA030553>